Monthly Notices of the ROYAL ASTRONOMICAL SOCIETY

MNRAS **447,** 2274–2281 (2015) doi:10.1093/mnras/stu2495

NuSTAR detection of a cyclotron line in the supergiant fast X-ray transient IGR J17544−2619

Varun Bhalerao,[1⋆] Patrizia Romano,[2] John Tomsick,[3] Lorenzo Natalucci,[4] David M. Smith,[5] Eric Bellm,[6] Steven E. Boggs,[3] Deepto Chakrabarty,[7] Finn E. Christensen,[8] William W. Craig,[3,9] Felix Fuerst,[6] Charles J. Hailey,[10] Fiona A. Harrison,[6] Roman A. Krivonos,[3] Ting-Ni Lu,[6,11] Kristin Madsen,[6] Daniel Stern,[12] George Younes[13] and William Zhang[14]

[1]*Inter University Centre for Astronomy and Astrophysics, PO Bag 4, Ganeshkhind, Pune 411007, India*
[2]*INAF, Istituto di Astrofisica Spaziale e Fisica Cosmica, Via U. La Malfa 153, I-90146 Palermo, Italy*
[3]*Space Sciences Laboratory, University of California, Berkeley, CA 94720, USA*
[4]*Istituto Nazionale di Astrofisica, INAF–IAPS, via del Fosso del Cavaliere, I-00133 Roma, Italy*
[5]*Physics Department and Santa Cruz Institute for Particle Physics, University of California, Santa Cruz, 1156 High St, Santa Cruz, CA 95064, USA*
[6]*Cahill Center for Astronomy and Astrophysics, Caltech, Pasadena, CA 91125, USA*
[7]*Kavli Institute for Astrophysics and Space Research, Massachusetts Institute of Technology, 70 Vassar Street, Cambridge, MA 02139, USA*
[8]*DTU Space, National Space Institute, Technical University of Denmark, Elektrovej 327, DK-2800 Lyngby, Denmark*
[9]*Lawrence Livermore National Laboratory, Livermore, CA 94550, USA*
[10]*Columbia Astrophysics Laboratory, Columbia University, New York, NY 10027, USA*
[11]*Institute of Astronomy, National Tsing Hua University, Hsinchu 30013, Taiwan*
[12]*Jet Propulsion Laboratory, California Institute of Technology, Pasadena, CA 91109, USA*
[13]*USRA, NSSTC, 320 Sparkman Drive, Huntsville, AL 35801, USA*
[14]*NASA Goddard Space Flight Center, Greenbelt, MD 20771, USA*

Accepted 2014 November 22. Received 2014 September 12; in original form 2014 June 30

ABSTRACT

We present *NuSTAR* spectral and timing studies of the supergiant fast X-ray transient (SFXT) IGR J17544−2619. The spectrum is well described by an ∼1 keV blackbody and a hard continuum component, as expected from an accreting X-ray pulsar. We detect a cyclotron line at 17 keV, confirming that the compact object in IGR J17544−2619 is indeed a neutron star. This is the first measurement of the magnetic field in an SFXT. The inferred magnetic field strength, $B = (1.45 \pm 0.03) \times 10^{12} G\,(1 + z)$ is typical of neutron stars in X-ray binaries, and rules out a magnetar nature for the compact object. We do not find any significant pulsations in the source on time-scales of 1–2000 s.

Key words: X-rays: binaries – X-rays: individual: IGR J17544-2619.

1 INTRODUCTION

High-mass X-ray binaries (HMXBs) are stellar systems composed of a compact object (either a neutron star or a black hole) and an early-type non-degenerate massive star primary. These systems are traditionally divided in two subclasses (e.g. Reig 2011, and references therein), depending on the nature of the primary that acts as a mass donor, and the mass-transfer and accretion mechanisms on to the compact object. While the Be/X-ray binaries (BeXBs) have main-sequence Be star primaries, and are only observed as transient sources showing bright outbursts lasting a few days, the OB supergiant binaries (SGXBs) are persistent systems with an evolved OB supergiant primary.

Among the ∼250 HMXBs known to populate our Galaxy and the Magellanic Clouds (Liu, van Paradijs & van den Heuvel 2005, 2006), a relatively small class termed supergiant fast x-ray transients (SFXTs) was recently recognized that shares properties with both BeXBs and SGXBs (Smith et al. 2004; in't Zand 2005; Sguera et al. 2005; Negueruela et al. 2006a). SFXTs are associated with OB supergiant stars but, unlike SGXBs, show the most dramatic manifestation of their activity as bright outbursts during which they experience an increase in X-ray luminosity by up to a factor of 10^5, reaching peak luminosities of 10^{36}–10^{37} erg s^{-1}. These bright outbursts last a few hours in the hard X-ray band (Sguera et al. 2005; Negueruela et al. 2006b) and, although the outbursts can last up to

⋆E-mail: varunb@iucaa.ernet.in

a few days in the soft X-ray band (e.g. Romano et al. 2007, 2013), they are still significantly shorter than those of typical BeXBs. The hard X-ray spectra, qualitatively similar to those of HMXBs that host accreting neutron stars (NS), are generally modelled with often heavily absorbed power laws with a high-energy cut-off. Therefore, it is tempting to assume that all SFXTs host an NS, even if pulse periods have only been measured for only a few systems. Currently, the SFXT class consists of 14 objects (see Romano et al. 2014, and references therein) and as many candidates (transients showing an SFXT behaviour but still lacking optical identification with an OB supergiant companion).

The physical mechanisms causing the bright SFXT outbursts are still uncertain. In the last decade, several models have been proposed that can be divided in two main groups, related to either the properties of the wind from the supergiant companion (in't Zand 2005; Sidoli et al. 2007; Walter & Zurita Heras 2007; Negueruela et al. 2008) or the properties of the compact object, in particular the presence of mechanisms regulating or inhibiting accretion (the propeller effect, Grebenev & Sunyaev 2007; Grebenev 2009; magnetic gating, Bozzo, Falanga & Stella 2008). A model of quasi-spherical accretion on to NS involving hot shells of accreted material above the magnetosphere (Shakura et al. 2014, and references therein) has recently been proposed.

The transient IGR J17544−2619 is the prototypical SFXT. It was discovered by *INTEGRAL* on 2003 September 17 (Sunyaev et al. 2003) during a 2-h flare that reached an 18–25 keV flux of 6×10^{-10} erg cm^{-2} s^{-1} (160 mCrab). This source was later observed in very bright states, lasting up to 10 h, with 20–40 keV fluxes up to 6×10^{-10} erg cm^{-2} s^{-1} (400 mCrab; Grebenev, Lutovinov & Sunyaev 2003; Grebenev et al. 2004; Sguera et al. 2006; Kuulkers et al. 2007; Walter & Zurita Heras 2007). Some flares were also found in archival *BeppoSAX* data (in't Zand et al. 2004). Several outbursts were also observed by *Swift* (Krimm et al. 2007; Sidoli et al. 2009a,b; Romano et al. 2011a,b; Farinelli et al. 2012) and *Suzaku*, which caught a $\gtrsim$ day long outburst (Rampy, Smith & Negueruela 2009).

IGR J17544−2619 is now a quite well-studied binary. The primary is an O9Ib star (Pellizza, Chaty & Negueruela 2006) at 3.6 kpc (Rahoui et al. 2008), and the orbital period is 4.926 ± 0.001 d (Clark et al. 2009; Smith 2014). While Drave et al. (2012) reported pulsations at 71.49 ± 0.02 s from the region around the source that they attributed to a spin period, Drave et al. (2014) did not confirm this detection.

IGR J17544−2619 is characterized by high variability. It was the first SFXT observed in detail during quiescence (at $L \sim 5 \times 10^{32}$ erg s^{-1}). A *Chandra* observation (in't Zand 2005) showed that the source is characterized by a very soft ($\Gamma = 5.9 \pm 1.2$) spectrum. Furthermore, this state of quiescence was followed by a bright flare, thus implying a dynamical range of at least four orders of magnitude. These observations, with their extreme luminosity changes occurring on such short time-scales, were interpreted in terms of accretion on to a compact object (probably an NS) from an inhomogeneous, or 'clumpy', wind from the supergiant companion (in't Zand 2005). Alternatively, Bozzo et al. (2008) explained the large luminosity swings observed on time-scales as short as hours in terms of transitions across the magnetic barriers. In this scenario, SFXTs with large dynamic range and $P_{\rm spin} \gtrsim 1000$ s must have magnetar-like fields ($B \gtrsim 10^{14}$ G).

In this paper, we present the first firm detection of a cyclotron line in the spectrum of an SFXT and hence the first direct measurement of its magnetic field.

Table 1. Observations of IGR J17544−2619.

	NuSTAR	
OBSID	30002003002	30002003003
Start date	2013-06-18T22:16:07	2013-06-19T09:31:07
End date	2013-06-19T09:31:07	2013-06-19T23:41:07
Start MJD	56461.9344668	56462.4059946
Exposure FPMA	17 533.22 s	26 238.50 s
Exposure FPMB	17 576.65 s	26 878.83 s
	Swift/XRT	
OBSID	00080201001	00080201003
Start date	2013-06-18T23:00:31	2013-06-19T00:42:08
End date	2013-06-18T23:20:55	2013-06-19T00:56:55
Start MJD	56461.9587016	56462.0292600
Exposure	1208.52 s	885.08 s

2 OBSERVATIONS AND ANALYSIS

IGR J17544−2619 was observed by *NuSTAR* on 2013 June 18–19, and near-simultaneously by *Swift* (Table 1). These observations were planned near orbital phase 0 (Smith 2014) to maximize a chance of detecting a flare.

NuSTAR data were extracted and reduced with NUSTARDAS v1.2.0 (14 June 2013), and HEASOFT 6.14. We extracted events from a 40-arcsec-radius circular region centred on the source. Background was extracted from a large source-free region on the same detector. Appropriate response matrices and ancillary response files for this observation were generated using `numkrmf` and `numkarf`, respectively. We used *NuSTAR* responses from CALDB version 20130509. *NuSTAR* consists of two co-aligned telescopes, each with a focal plane module (FPMA and FPMB). In FPMB, the source position was strongly contaminated by stray light of nearby bright sources during OBSID 30002003002. IGR J17544−2619 showed flaring activity during this observation (Section 4).

The *Swift*/XRT data were processed with standard procedures (XRTPIPELINE v0.12.8), filtering and screening criteria using FTOOLS (v6.15.1). Source events were accumulated within a circular region with a radius of 20 pixels (1 pixel ∼2.36 arcsec). Background events were accumulated from an annular source-free region centred on IGR J17544−2619 (inner/outer radii of 70/100 pixels). For our spectral analysis, ancillary response files were generated with XRTMKARF to account for different extraction regions, vignetting, and PSF corrections. We used the latest XRT spectral redistribution matrices in CALDB (20140120).

Data were analysed in XSPEC (v12.8.1). We used *Swift*/XRT data from 0.3 to 10 keV and *NuSTAR* data in the energy range 3–50 keV. Data were grouped to have at least 20 source+background photons per bin, and χ^2 statistics were used for fitting. We used atomic cross-sections from Verner et al. (1996) and elemental abundances from Wilms, Allen & McCray (2000).

3 TIMING

Fig. 1 shows the background-subtracted light curves with 50 s bins for both FPMs for the entire observation. OBSID 30002003002 shows strong flaring activity from IGR J17544−2619, with a bright flare that is about 10 times stronger than the average flux level (Section 4). The source is less variable in OBSID 30002003003, with a dynamic range of just a factor of 2. The average absorbed source flux in this OBSID is $(1.11 \pm 0.01) \times 10^{-11}$ erg cm^{-2} s^{-1} in

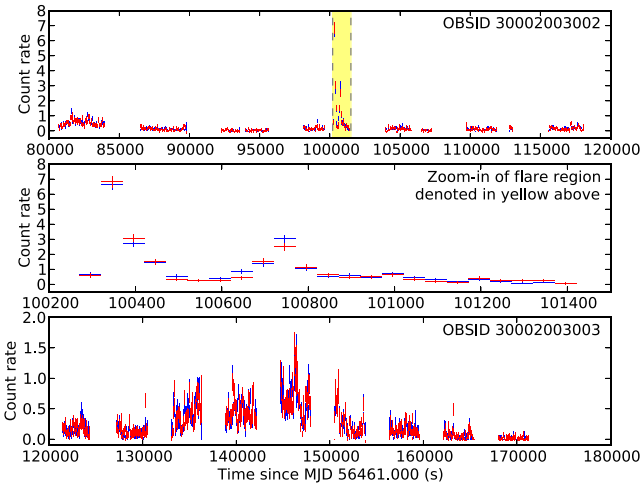

Figure 1. Background-subtracted *NuSTAR* light curves of IGR J17544−2619 OBSID 30002003002 (top panel) and OBSID 30002003003 (bottom panel). The middle panel zooms in on the flare region from OBSID 30002003002. Blue and red plus signs show count rates in 50 s bins for the focal plane modules FPMA and FPMB, respectively. For all panels, the *X*-axis is time since MJD 56461.0, *Y*-axes show counts s^{-1} in the 3–50 keV band. For reference, the average flux in OBSID 30002003003 in the entire 3–50 keV band is $(3.53 \pm 0.05) \times 10^{-11}$ erg cm^{-2} s^{-1} (1 mCrab).

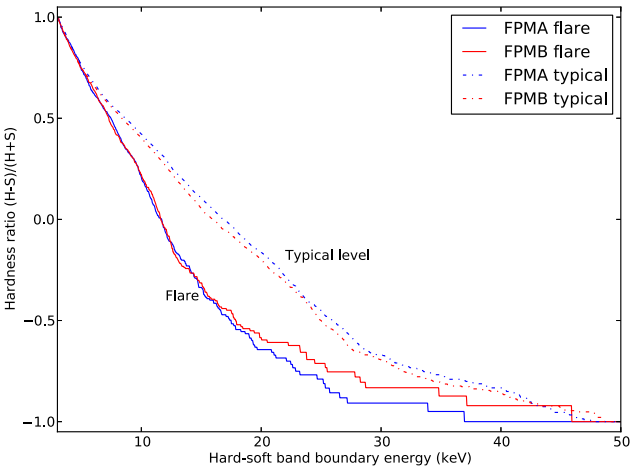

Figure 2. Hardness ratio of IGR J17544−2619 as a function of energy, during the flare and in quiescence. For each energy *E*, we define the 3 − *E* keV band as the soft band, and *E* − 50 keV band as the hard band. The *Y*-axis shows the hardness ratio, defined as (H−S)/(H+S). Red curves are for FPMA, and blue curves are for FPMB. The solid lines are cumulative fluxes of the flare (Fig. 1), compared with quiescent fluxes from OBSID 30002003003. The flare is softer than the 'typical' state, the difference being most prominent at 15–20 keV. For example, with 3–15 keV and 15–50 keV bands, the hardness ratio is about 0.1 in the typical state, but falls to about −0.3 during the flare.

the 3–10 keV band, consistent with the average unabsorbed source flux of 10^{-11} erg cm^{-2} s^{-1} measured by *Swift*/XRT in the 2–10 keV band (Romano et al. 2011a). The total absorbed flux observed by *NuSTAR* is $(3.53 \pm 0.05) \times 10^{-11}$ erg cm^{-2} s^{-1}in the 3–50 keV band.

We searched the *NuSTAR* data for any pulsations in IGR J17544−2619. No strong peaks are seen in the power spectra. An epoch folding search does not yield any strong periodicity either. In particular, we do not detect the claimed 71.49 ± 0.02 s pulsation (Drave et al. 2012). Further, we computed a power spectrum and renormalized it relative to the local mean power in order to search for statistically significant periodic signals. We found periodic signals at about 1455 and 1940 s, which are integer fractions of the spacecraft's orbital period. The instrumental origin was confirmed when we extracted photons from background regions far from the source, and found peaks at the same periods. We conclude that IGR J17544−2619 does not show any strong pulsations in the range of 1 s to about 2000 s, consistent with Drave et al. (2014).

4 FLARE

IGR J17544−2619 is known for strong flaring behaviour. *NuSTAR* detected a flare during OBSID 30002003002, starting approximately at MJD 56462.161 and spanning about 220 s (Fig. 1, middle panel). It was followed by a smaller flare about 400 s later. The spectrum of the first flare is relatively flat from 3 to 10 keV and falls off at higher energies. We calculate the model-independent flux for the source and the flare using *NuSTAR* response files. The average absorbed flux in the flare is $(3.1 \pm 0.1) \times 10^{-10}$ erg cm^{-2} s^{-1} (9 mCrab) in the 3–50 keV range, about an order of magnitude higher than the average flux of $(3.54 \pm 0.05) \times 10^{-11}$ erg cm^{-2} s^{-1} (1 mCrab) measured in OBSID 30002003003. This is consistent with typical flares observed near periastron from this source (Romano et al. 2011a). The source becomes softer during the flare (Fig. 2). The average absorbed flux of the second flare is $(1.5 \pm 0.1) \times 10^{-10}$ erg cm^{-2} s^{-1}.

Broad-band (∼0.2–60 keV) flare spectra (∼10^{-9} erg cm^{-2} s^{-1}) are typically modelled as an absorbed cut-off power-law or an absorbed power-law with an exponential cut-off. For example, Rampy et al. (2009) fit the *Suzaku* XIS+PIN data on the 2008 March 31 outburst with an absorbed power-law with an exponential cut-off with $\Gamma = 0.9$, and $E_{\rm fold} = 10.5$ keV; Romano et al. (2011a) adopt an absorbed power-law with a high-energy cut-off for the *Swift* BAT+XRT data on the 2009 June 6 outburst and find $\Gamma = 0.6$, $E_{\rm cut} = 3.3$ keV, and $E_{\rm fold} = 8.1$ keV. However, our flare data are not fitted well by a simple absorbed blackbody or absorbed cut-off power-law model, which give $\chi^2_\nu = 1.76$ and 1.4 with 47 and 46 degrees of freedom, respectively. The simplest model for the flare spectrum is an unabsorbed power–law with two breaks (`bkn2pow`) at 8.9 and 11.1 keV. For this model, we get $\chi^2_\nu = 0.93$ with 44 degrees of freedom.

5 SPECTRUM

For spectral modelling, we only use data from OBSID 30002003003, where the source is in a steady state. We used *NuSTAR* data extracted with a 40 arcsec extraction region, grouped to make bins of at least 20 photons and *Swift*/XRT data from both *Swift* observations. The spectrum can be fit by a two-component model consisting of an ∼1 keV blackbody and a harder, non-thermal component (Fig. 3). This non-thermal component can be interpreted as a Comptonized spectrum with seed photons from the blackbody – indeed, a non-thermal Comptonization model (`nthcomp`) with $\Gamma = 1.2$ and $kT_{\rm e} = 5.7$ keV gives a reasonable fit (Table 2). Alternately, this component is also fitted well by the empirical cut-off power-law model with $\Gamma = -1.1$ and $E_{\rm cut} = 6.7$ keV (Table 3). Hereafter, we refer to these as continuum models I and II, respectively.

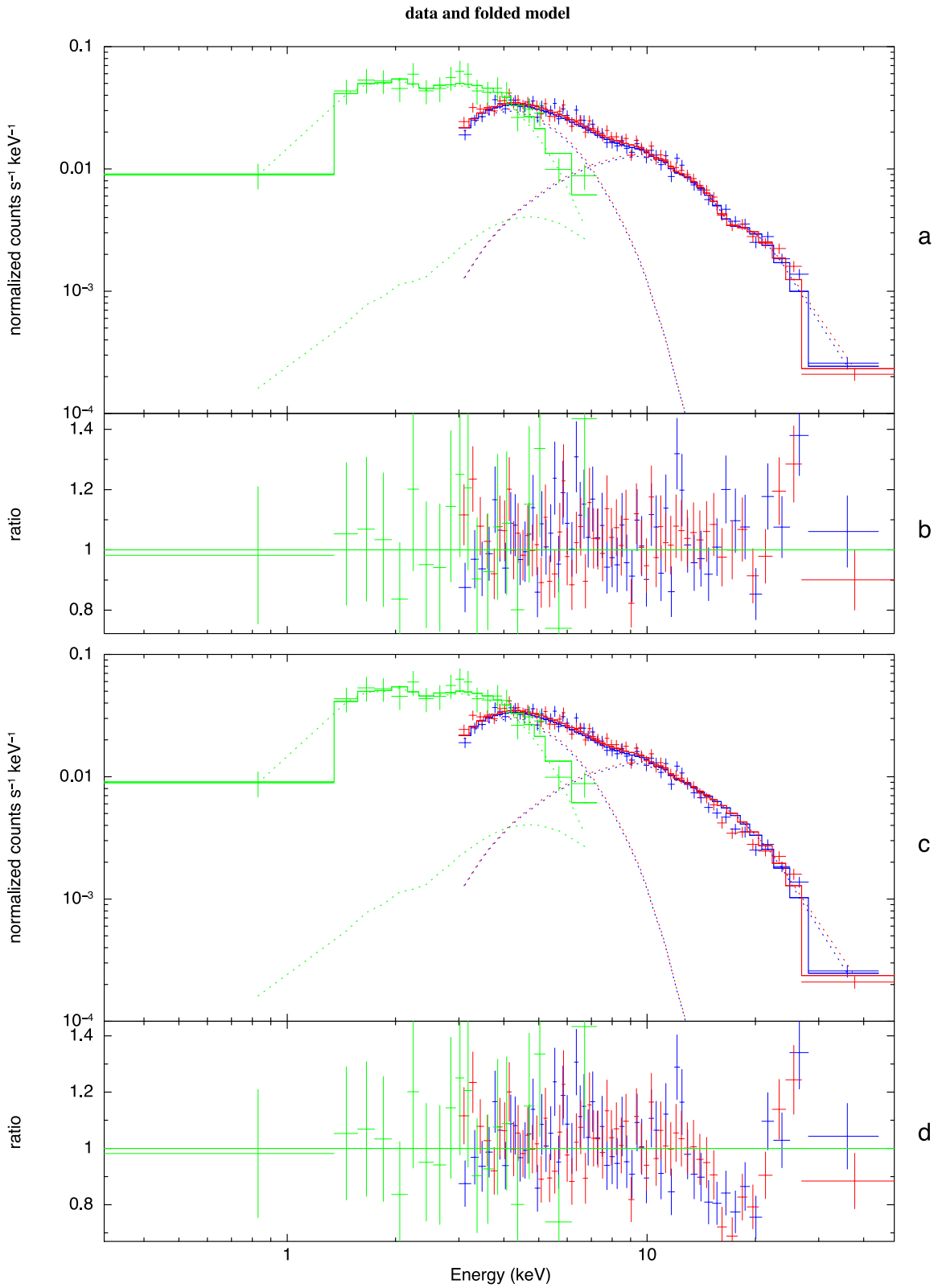

Figure 3. Joint fit to *NuSTAR* and *Swift*/XRT data with `bbodyrad + nthcomp` as the continuum model. Blue, red and green symbols denote data from *NuSTAR* FPMA, *NuSTAR* FPMB, and *Swift*/XRT, respectively. For plotting *NuSTAR* data have been re-binned to a minimum SNR 10 in each bin-actual fitting was done with smaller bins with at least 20 photons each for both: *NuSTAR* and *Swift*/XRT. We allow a scaling factor between *NuSTAR* FPMA, FPMB, and *Swift*/XRT fluxes. Panel (a) shows the best fit with the continuum and a single cyclotron line (no harmonics). The ratio data to the model (panel b) is relatively flat, as expected for a well-fitted model. Panel (c) shows the same model with the cyclotron line deleted (but without refitting). The ratio of data to the model (panel d) clearly show the cyclotron line.

Table 2. Spectral fits for IGR J17544−2619 with continuum model I (`bbodyrad + nthcomp`).

Model component	Parameter name	Model: No line	Single line	Line + harmonic	Two lines
		Continuum parameters			
N_H	(10^{22} cm^{-2})	1.7 ± 0.3	1.52 ± 0.28	1.43 ± 0.28	1.45 ± 0.28
bbodyrad	kT (keV)	0.95 ± 0.04	1.04 ± 0.02	1.07 ± 0.03	1.06 ± 0.04
	norm	1.06 ± 0.17	0.92 ± 0.10	0.83 ± 0.11	$0.85^{+0.10}_{-0.06}$
nthcomp	Γ^a	1.21 ± -0.05	$1.00^{+0.03}_{-***}$	$1.00^{+0.06}_{-***}$	$1.00^{+0.05}_{-***}$
	kT_e (keV)	5.66 ± 0.24	5.04 ± 0.08	$6.4^{+6.2}_{-0.9}$	$5.8^{+5.5}_{-0.5}$
	norm (10^{-6})	94 ± 29	$4.0^{+18}_{-0.2}$	$3.1^{+50}_{-0.5}$	$3.4^{+64}_{-0.8}$
X-norm constant	FPMB	1.12 ± 0.02	1.12 ± 0.02	1.12 ± 0.02	1.12 ± 0.02
	Swift/XRT	1.33 ± 0.09	1.34 ± 0.09	1.35 ± 0.09	1.35 ± 0.09
		Cyclotron lines			
Line 1	Energy (keV)	–	16.9 ± 0.3	16.9 ± 0.3	17.0 ± 0.3
	Width (keV)	–	1.6 ± 0.6	3.5 ± 1.0	3.0 ± 0.8
	Depth (keV)	–	0.40 ± 0.07	$0.58^{+0.06}_{-0.14}$	$0.53^{+0.06}_{-0.09}$
Line 2	Energy (keV)	–	–	$(33.8)^b$	$32.9^{+1.3}_{-1.1}$
	Width (keV)	–	–	9.8 ± 5.0	$6.6^{+6.6}_{-2.0}$
	Depth (keV)	–	–	$1.2^{+1.4}_{-0.6}$	0.9 ± 0.4
		Quality of fit			
Degrees of freedom		503	500	498	497
χ^2		515.9	477.2	467.7	467.1
$\Delta\chi^2$		–	−38.7	−48.2	−48.8

Notes. We allow relative scaling of *NuSTAR* FPMA, FPMB, and *Swift*/XRT data. The best-fitting values for the cross-normalization (X-norm) constants are included in the table.
[a]In fits including the cyclotron lines, Γ gets pegged at its lower limit of 1.0. Hence we give only one-sided error bars on this parameter.
[b]Energy of the harmonic is defined as two times the energy of the fundamental, and is not a free parameter.

We can calculate the size of the emitting area of the blackbody component from its normalization (norm[1] in XSPEC) and distance to the object: norm $= R^2_{\rm km}/D^2_{10}$. Using a nominal distance of 3.6 kpc to IGR J17544−2619 (Rahoui et al. 2008) and assuming a circular emitting area, the best-fitting norm values correspond to a radius $R \approx 0.3$ km. This is consistent with the size of an accretion hotspot on the NS for low accretion rates (Frank, King & Raine 2002).

Regardless of the continuum model, the fits show systematic residuals mimicking absorption features. Good fits can be obtained only on introducing cyclotron absorption features in the model (Fig. 3). We tested the presence and significance of these lines with various extraction apertures and binning methods. Further, we also tested the presence of a harmonic in two ways: enabling the harmonic in `cyclabs`, and adding an independent line at higher energy. All these tests gave consistent results: the spectral fits are significantly better when a cyclotron line is included in the spectral model. The fits improve further when the cyclotron line harmonic is also added in the fit. Adding an independent higher energy line gives results broadly consistent with the location of a harmonic.

In continuum model I, adding a cyclotron line gives $\Delta\chi^2 = 38.7$ for 3 more degrees of freedom. The best-fitting line energy is $E_{\rm cyc} = 16.9 \pm 0.3$ keV (Table 2). For continuum model II, adding a cyclotron line gives $\Delta\chi^2 = 42.6$ for 3 more degrees of freedom (Table 3). The best-fitting line energy, $E_{\rm cyc} = 16.8 \pm 0.3$ keV, agrees with the fit for model I. In both cases, adding a harmonic decreases the χ^2 further. If we introduce a second, independent absorption feature, its best-fitting energy agrees with the expected harmonic to within 1σ for continuum model I. For continuum model II, the best-fitting energy of this absorption feature is slightly lower than twice the fundamental. This slight difference in energies is seen in other X-ray binaries as well (Caballero & Wilms 2012).

We checked for the significance of the line depth using three methods for both continuum models. We consider the case with only the fundamental line without any harmonics. We allow the line depth to vary over a wide range, so as to search for cyclotron absorption or emission features. (i) *F-test*: based on the improvement in χ^2 by adding the line, we can calculate a false detection probability for the line.[2] For continuum model I, we get $p = 1.7 \times 10^{-8}$ while for continuum model II, $p = 2.3 \times 10^{-9}$. (ii) *Non-zero line depth*: we considered models with the fundamental line only, and stepped through a grid of values of the line depth and width with the XSPEC command `steppar`, and noted the change in χ^2. For continuum model I, we find that changing the line depth to zero gives a minimum $\Delta\chi^2$ of 52, corresponding to a 7σ detection. The constraints were even stronger for continuum model II. (iii) *Monte Carlo simulations*: further, we tested the line significance by simulating spectra using the XSPEC script `simftest`. We used the continuum model II, consisting of a blackbody and a cut-off power-law as our *null hypothesis*. We simulated fake spectra from this model and fitted them with (a) only continuum, and (b) continuum + cyclotron line. To improve the speed and convergence of the fits, we performed simulations using only the two *NuSTAR*

[1] http://heasarc.gsfc.nasa.gov/xanadu/xspec/manual/XSmodelBbodyrad.html

[2] Note that the line depth was allowed to be positive as well as negative, so that the null model (no line) is not a boundary case for the *F*-test.

Table 3. Spectral fits for IGR J17544−2619 with continuum model II (`bbodyrad + cutoffpl`).

Model component	Parameter name	Model: No line	Single line	Line + harmonic	Two lines
		Continuum parameters			
N_H	(10^{22} cm^{-2})	1.6 ± 0.3	1.38 ± 0.26	1.34 ± 0.22	1.4 ± 0.2
bbodyrad	kT (keV)	0.99 ± 0.04	$1.097^{+0.02}_{-0.006}$	$1.115^{+0.03}_{-0.006}$	$1.102^{+0.02}_{-0.006}$
	norm	$1.04^{+0.17}_{-0.12}$	0.78 ± 0.08	0.74 ± 0.08	0.76 ± 0.07
cutoffpl	Γ^a	$-1.1^{+0.3}_{-0.2}$	$-3.0^{+0.4}_{-***}$	$-2.8^{+1.7}_{-***}$	$-3.0^{+0.4}_{-***}$
	E_{cut} (keV)	$6.6^{+0.7}_{-0.5}$	$4.04^{+0.02}_{-0.05}$	$4.75^{+0.03}_{-0.5}$	$4.18^{+0.02}_{-0.08}$
	norm (10^{-6})	21^{+13}_{-8}	$0.72^{+0.01}_{-0.04}$	$0.54^{+0.02}_{-0.14}$	0.67 ± 0.02
X-norm constant	FPMB	1.12 ± 0.02	1.12 ± 0.02	1.12 ± 0.02	1.12 ± 0.02
	Swift/XRT	1.34 ± 0.09	1.35 ± 0.09	1.35 ± 0.08	1.35 ± 0.08
		Cyclotron lines			
Line 1	Energy (keV)	–	16.8 ± 0.3	$16.6^{+0.2}_{-0.3}$	$16.9^{+0.2}_{-0.3}$
	Width (keV)	–	$2.6^{+0.6}_{-0.3}$	$4.6^{+0.8}_{-0.3}$	$3.1^{+0.6}_{-0.3}$
	Depth (keV)	–	$0.49^{+0.06}_{-0.04}$	$0.72^{+0.18}_{-0.03}$	$0.54^{+0.20}_{-0.04}$
Line 2	Energy (keV)	–	–	$(33.2)^b$	$30.0^{+1.9}_{-0.5}$
	Width (keV)	–	–	$7.4^{+4.3}_{-3.5}$	$1^{+7}_{-***}{}^c$
	Depth (keV)	–	–	1.09 ± 0.10	$0.7^{+0.2}_{-0.3}$
		Quality of fit			
Degrees of freedom		503	500	498	497
χ^2		516.0	473.4	467.4	465.3
$\Delta\chi^2$		0.0	−42.6	−48.6	−50.7

Notes. We allow relative scaling of *NuSTAR* FPMA, FPMB, and *Swift*/XRT data. The best-fitting values for the cross-normalization (X-norm) constants are included in the table.
[a]In fits including the cyclotron lines, Γ gets pegged at its lower limit of −3.0. Hence we give only one–sided error bars on this parameter.
[b]Energy of the harmonic is defined as two times the energy of the fundamental, and is not a free parameter.
[c]The minimum width of line 2 gets pegged at its lower limit of 1 keV before obtaining $\Delta\chi^2 = 1.0$, so we do not give a lower limit.

modules, fixing the column density to the value found when XRT was included. We repeated this test 1000 times and noted the change in χ^2 obtained by adding a cyclotron line of similar width (within the 90 per cent confidence region obtained with the actual data). Since the cyclotron line adds three free parameters, we expect that the histogram of $\Delta\chi^2$ values should follow a χ^2 distribution with three degrees of freedom. This is indeed the case, as seen in Fig. 4. The highest $\Delta\chi^2$ obtained in our simulation is 18.7, significantly lower than $\Delta\chi^2 = 41.2$ obtained in real data. We estimate that 10^7–10^8 simulations would be required to get $\Delta\chi^2 > 40$ in one of them. Performing such a large number of simulations is technically infeasible. However, scaling from our 1000 simulations, we obtain a line significance of $>5\sigma$. We repeated this test with continuum model I. The observed $\Delta\chi^2$ for this model is 37.1, but the maximum value we obtain in 1000 simulations is 12, confirming the high significance of the cyclotron line.

We tested the presence of a line at 8.5 keV by adding a model component with half the energy and half the width as the 17 keV line. We do not detect any significant absorption near 8.5 keV, with 3σ limits on line depth as $D^{\rm I}_{8.5} < 0.19$ and $D^{\rm II}_{8.5} < 0.15$ for continuum models I and II, respectively.

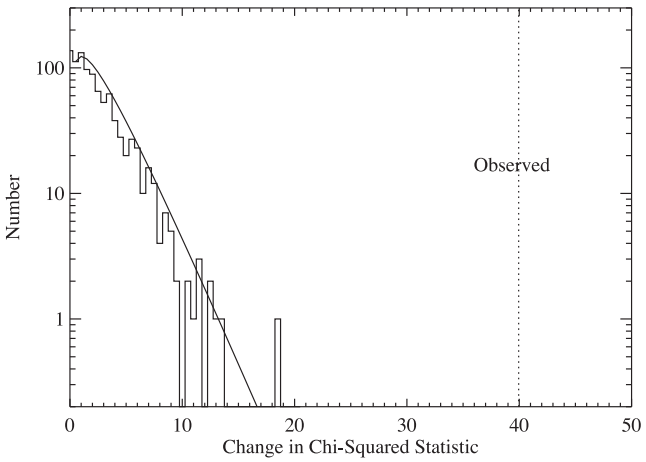

Figure 4. Results of Monte Carlo simulations for testing line significance for continuum model II (Section 5). We simulated 1000 fake *NuSTAR* spectra for the continuum-only model (`bbodyrad + cut-offpl`), and attempted to fit them with a continuum+line model with N_H fixed at the value obtained with a joint *Swift*/XRT fit. The solid histogram shows $\Delta\chi^2$ values obtained in the simulations, and the smooth curve is a χ^2 distribution with 3 degrees of freedom. The $\Delta\chi^2$ attained in actual data (dashed vertical line) is significantly higher than values attained in simulations. This $\Delta\chi^2$ value differs that in Table 3 due to the simplifying assumptions made in these simulations (Section 5).

6 DISCUSSION

Despite a decade of investigation, the mechanisms responsible for the flaring behaviour of SFXTs are still far from certain. Several, non-mutually-exclusive, models have been proposed, depending on

the donor star wind and/or the accreting NS properties. For the 'clumpy wind' models (in't Zand 2005; Sidoli et al. 2007; Walter & Zurita Heras 2007; Negueruela et al. 2008), the common key parameters are the geometry and inhomogeneity of the stellar wind from the supergiant donor star. For the 'gating' models, mechanisms are required to regulate or inhibit accretion (the propeller effect – see Grebenev & Sunyaev 2007; or magnetic gating – see Bozzo et al. 2008). In particular, in the magnetic gating model (Bozzo et al. 2008, and references therein), the large intensity swings observed in IGR J17544−2619 are explained in terms of slowly rotating ($P_{\rm spin} \gtrsim 1000$ s) magnetar ($B \gtrsim 10^{14}$ G) and a switch on/off of the source due to the propeller effect. The quasi-spherical accretion model (Shakura et al. 2014, and references therein), on the other hand, featuring hot shells of accreted gas above the magnetosphere of a slowly rotating ($P_{\rm spin} \gtrsim 1000$ s) NS, can be applied to the bright fast flares of SFXTs even without invoking magnetar-like B fields, when the mass accretion rate increases due to the sporadic capture of magnetized stellar wind plasma.

It is clear that knowledge of the magnetic field is a powerful discriminator among various models. Until now, however, no measurements of the cyclotron lines were available, hence the magnetic field could only be estimated indirectly from the empirical relationship of Coburn et al. (2002), using the cut-off energy derived from spectral fitting as a proxy for the magnetic field (B). For SFXTs, the typical cut-off energies are at about 10–20 keV, so the estimated magnetic fields range from 2×10^{12} G for XTE J1739.1−302, to about (2–3) $\times 10^{12}$ G for IGR J17544−2619 (Sidoli et al. 2009b), and $\lesssim 3 \times 10^{12}$ G for AX J1841.0−0536 (Romano et al. 2011b).

Detections of cyclotron features in HMXBs are still scarce, with under 20 confirmed detections before *NuSTAR* (Caballero & Wilms 2012). Among those is the cyclotron line at 33 ± 4 keV reported in the *candidate* SFXT IGR J16493−4348 (D'Aì et al. 2011), implying $B \approx 4 \times 10^{12}$ G. Our *NuSTAR* spectrum provides the very first measurement of such a feature in a confirmed SFXT, the prototype of the class IGR J17544−2619, at 16.8 ± 0.3 keV. Our data also show hints of a line harmonic at an energy consistent with twice the fundamental, though slightly lower values are preferred (Tables 2 and 3). The observed energy of cyclotron lines depends on the local magnetic field and the gravitational redshift caused by the NS:

$$B_{12} = \frac{E_{\rm cyc}}{11.6\,{\rm keV}}(1+z), \quad (1)$$

where B_{12} is the magnetic field in units of 10^{12} G. Hence, we conclude that the compact object in IGR J17544−2619 is indeed an NS, with magnetic field strength $B = (1.45 \pm 0.03) \times 10^{12}$ G $(1 + z)$. The gravitational redshift factor $(1 + z)$ is typically in the range of 1.25–1.4 for NS (Caballero & Wilms 2012), but may be a bit higher for IGR J17544−2619 due to the higher mass of the NS (Bhalerao 2012). This B value is consistent with the $B \lesssim 3 \times 10^{12}$ G constraint from spectral modelling (Sidoli et al. 2009b).

An alternate interpretation is that the feature is a proton cyclotron line. In this latter case, the inferred magnetic field strength is $B'_{12} = (m_{\rm p}/m_{\rm e})B_{12}$, where $m_{\rm p}$ and $m_{\rm e}$ are proton and electron masses, respectively. This corresponds to a magnetic field strength $B' = (2.66 \pm 0.06) \times 10^{15}$ G $(1 + z)$. In such fields, the equivalent width of lines is expected to be very low – just few eV – due to vacuum polarization (Ho & Lai 2003, but also see Tiengo et al. 2013). This contrasts strongly with the measured 2.2 keV equivalent width of the fundamental. Further, this latter magnetic field also contradicts the constraint from Sidoli et al. (2009b). As a result, we rule out this possibility that this absorption feature is a proton cyclotron line.

The energy of the cyclotron line, and the inferred magnetic field of IGR J17544−2619 is comparable to typical values measured in other X-ray binaries (Caballero & Wilms 2012). Furthermore, cyclotron line harmonics tend to have energies slightly lower than the corresponding multiple of the fundamental (Caballero & Wilms 2012) – as seen in our data, too.

Thus, the NS in IGR J17544−2619 is definitely not a magnetar, implying that one of the key requirements of the magnetic gating model is not met. Such a low value of the magnetic field strength, however is compatible with the centrifugal gating and quasi-spherical settling accretion models.

ACKNOWLEDGEMENTS

This work was supported in part under NASA Contract no. NNG08FD60C, and made use of data from the *NuSTAR* mission, a project led by the California Institute of Technology, managed by the Jet Propulsion Laboratory, and funded by the National Aeronautics and Space Administration. We thank the *NuSTAR* Operations, Software and Calibration teams as well as the *Swift* team for support with the execution and analysis of these observations. This research has made use of the *NuSTAR* Data Analysis Software (NUSTARDAS) jointly developed by the ASI Science Data Center (ASDC, Italy) and the California Institute of Technology (USA). PR acknowledges contract ASI-INAF I/004/11/0. LN wishes to acknowledge the Italian Space Agency (ASI) for Financial support by ASI/INAF grant I/037/12/0-011/13. VB thanks Dipankar Bhattacharya for helpful discussions.

Facilities: NuSTAR, *Swift*.

REFERENCES

Bhalerao V. B., 2012, PhD thesis, California Institute of Technology, available at: http://resolver.caltech.edu/CaltechTHESIS:05312012-150403422

Bozzo E., Falanga M., Stella L., 2008, ApJ, 683, 1031

Caballero I., Wilms J., 2012, Mem. Soc. Astron. Ital., 83, 230

Clark D. J., Hill A. B., Bird A. J., McBride V. A., Scaringi S., Dean A. J., 2009, MNRAS, 399, L113

Coburn W., Heindl W. A., Rothschild R. E., Gruber D. E., Kreykenbohm I., Wilms J., Kretschmar P., Staubert R., 2002, ApJ, 580, 394

D'Aì A., Cusumano G., La Parola V., Segreto A., Di Salvo T., Iaria R., Robba N. R., 2011, A&A, 532, A73

Drave S. P., Bird A. J., Townsend L. J., Hill A. B., McBride V. A., Sguera V., Bazzano A., Clark D. J., 2012, A&A, 539, A21

Drave S. P., Bird A. J., Sidoli L., Sguera V., Bazzano A., Hill A. B., Goossens M. E., 2014, MNRAS, 439, 2175

Farinelli R. et al., 2012, MNRAS, 424, 2854

Frank J., King A., Raine D. J., 2002, Accretion Power in Astrophysics. Cambridge Univ. Press, Cambridge

Grebenev S., 2009, Proc. The Extreme Sky: Sampling the Universe Above 10 keV (PoS(extremesky2009)060), Supergiant Fast X-ray Transients observed by INTEGRAL, available at: http://pos.sissa.it/archive/conferences/096/060/extremesky2009_060.pdf

Grebenev S. A., Sunyaev R. A., 2007, Astron. Lett., 33, 149

Grebenev S. A., Lutovinov A. A., Sunyaev R. A., 2003, Astron. Telelegram, 192, 1

Grebenev S. A., Rodriguez J., Westergaard N. J., Sunyaev R. A., Oosterbroek T., 2004, Astron. Telelegram, 252, 1

Ho W. C. G., Lai D., 2003, MNRAS, 338, 233

in't Zand J. J. M., 2005, A&A, 441, L1

in't Zand J., Heise J., Ubertini P., Bazzano A., Markwardt C., 2004, in Schoenfelder V., Lichti G., Winkler C., eds, ESA SP-552: 5th INTEGRAL Workshop on the INTEGRAL Universe. ESA, Noordwijk, p. 427

Krimm H. A. et al., 2007, Astron. Telelegram, 1265, 1
Kuulkers E. et al., 2007, Astron. Telelegram, 1266, 1
Liu Q. Z., van Paradijs J., van den Heuvel E. P. J., 2005, A&A, 442, 1135
Liu Q. Z., van Paradijs J., van den Heuvel E. P. J., 2006, A&A, 455, 1165
Negueruela I., Smith D. M., Reig P., Chaty S., Torrejón J. M., 2006a, in Wilson A., ed., ESA SP-604: Proc. the X-ray Universe 2005. ESA, Noordwijk, p. 165
Negueruela I., Smith D. M., Harrison T. E., Torrejón J. M., 2006b, ApJ, 638, 982
Negueruela I., Torrejón J. M., Reig P., Ribó M., Smith D. M., 2008, in Bandyopadhyay R. M., Wachter S., Gelino D., Gelino C. R., eds, AIP Conf. Proc. 1010, A Population Explosion: The Nature & Evolution of X-ray Binaries in Diverse Environments. Am. Inst. Phys., New York, p. 252
Pellizza L. J., Chaty S., Negueruela I., 2006, A&A, 455, 653
Rahoui F., Chaty S., Lagage P.-O., Pantin E., 2008, A&A, 484, 801
Rampy R. A., Smith D. M., Negueruela I., 2009, ApJ, 707, 243
Reig P., 2011, Ap&SS, 332, 1
Romano P., Sidoli L., Mangano V., Mereghetti S., Cusumano G., 2007, A&A, 469, L5
Romano P. et al., 2011a, MNRAS, 410, 1825
Romano P. et al., 2011b, MNRAS, 412, L30
Romano P. et al., 2013, Adv. Space Res., 52, 1593
Romano P. et al., 2014, A&A, 562, A2
Sguera V. et al., 2005, A&A, 444, 221
Sguera V. et al., 2006, ApJ, 646, 452
Shakura N., Postnov K., Sidoli L., Paizis A., 2014, MNRAS, 442, 2325
Sidoli L., Romano P., Mereghetti S., Paizis A., Vercellone S., Mangano V., Götz D., 2007, A&A, 476, 1307
Sidoli L. et al., 2009a, MNRAS, 397, 1528
Sidoli L. et al., 2009b, ApJ, 690, 120
Smith D. M., 2014, Astron. Telegram, 6227, 1
Smith D. M., Negueruela I., Heindl W. A., Markwardt C. B., Swank J. H., 2004, BAAS, 36, 954
Sunyaev R. A., Grebenev S. A., Lutovinov A. A., Rodriguez J., Mereghetti S., Gotz D., Courvoisier T., 2003, Astron. Telelegram, 190, 1
Tiengo A. et al., 2013, Nature, 500, 312
Verner D. A., Ferland G. J., Korista K. T., Yakovlev D. G., 1996, ApJ, 465, 487
Walter R., Zurita Heras J., 2007, A&A, 476, 335
Wilms J., Allen A., McCray R., 2000, ApJ, 542, 914

This paper has been typeset from a TEX/LATEX file prepared by the author.